Methods to estimate the number of surface nucleation sites on glass particles

Eduardo B. Ferreira[1]

Vitrovita Instituto de Inovação em Vitrocerâmicos, Rua Alfredo Lopes, 1717, E12, 13.560-460, São Carlos, SP, Brazil

Marcio L. F. Nascimento, Hugo Stoppa & Edgar D. Zanotto

LaMaV – DEMa / UFSCar, Rod. Washington Luiz, Km. 235, 13565-905, São Carlos, SP, Brazil

Based on the Johnson–Mehl–Avrami–Kolmogorov (JMAK) theory, we propose two new models to describe the crystallisation kinetics of glass particles and use them to determine the density of nucleation sites, N_s, on glass powders. We tested these models with sintered compacts of diopside glass particles using sinter-crystallisation treatments at 825°C (T_g~727°C), that covered from null to almost 100% crystallised volume fraction. We measured and compared the evolution of the crystallised volume fractions by optical microscopy and x-ray diffraction. Then we fit our expressions to experimental data using N_s and R (the average particle radius) as adjustable parameters. For comparison, we also fit to our data existing expressions that describe the crystallised volume fraction in glass powders. We demonstrate that all the methods allow one to estimate N_s with reasonable accuracy. For our ground and water washed diopside glass powder, N_s is between 10^{10}–10^{11} sites.m^{-2}. The reasonable agreement between experimental and adjusted R confirms the consistency of all five models tested. However, one of our equations does not require taking into account the change of crystallisation mode from 3-dimensional to 1-dimensional, and this is advantageous.

1. Introduction

Viscous flow sintering of glass powder compacts with simultaneous or subsequent surface crystallisation is an exciting alternative for the development of new glass-ceramics[1–2] because this method avoids the search for and complications that appear when adding nucleating agents. However, it is quite challenging to simulate and model[3] these two complex processes due to the difficulty of measuring some key parameters that control the crystallisation kinetics, such as the surface density of nucleation sites, N_s.

In the vast majority of glasses, crystallisation starts on athermal surface sites, such as scratches, solid impurities, etc. In this case, the kinetics of overall crystallisation of monodispersed spherical glass particles was long ago treated by Mampel[4] and Todes,[5] but no analytical solution is available so far.

Muller's[6] approach for the crystallisation kinetics of glass powders considers cuboidal crystals growing at a rate u on the surface and towards the interior of cubic particles of edge $2R$. If $2d$ is the distance between neighbouring nucleation sites, for $R>d$ Muller[6]

obtained the following approximation for the first stage of 3-dimensional crystal growth

$$\alpha(t) = \frac{B}{8}\left(\frac{ut}{R}\right)^3 \tag{1}$$

where $\alpha(t)$ is the crystallised volume fraction and t is the treatment time. Considering further that the nucleation sites are regularly distributed on the vertices, edges and faces of the cubic particles, B is given by

$$B = 24\left[\frac{R}{d} - \frac{1}{2}\right]^2 + 2 \tag{2}$$

Such crystals can grow on the glass particle surfaces up to a maximum length $r_m = ut_m = d$, when they impinge at time t_m. Subsequent growth would follow the kinetics given by

$$\alpha(t) = 1 - \left(1 - \frac{ut}{R}\right)^3 \tag{3}$$

Kinetics expressed by Equation (3) are observed when the crystal/glass boundaries move at constant velocity, u, and the reaction product has neither a retarding nor a catalytic effect, i.e. the reaction rate is constant. This equation is known as "Jander's law"[7,8] and is

[1] Corresponding author, now at the Sao Paulo State University, DMT/FEG, Guaratingueta/SP. Email ebferreira@feg.unesp.br

not valid for time intervals such that $(ut)/R > 1$.

For $R < d$, Muller[6] developed an expression for the crystallisation kinetics considering that not all particles in the sample have surface nucleation sites, but some have only a single site that is located on a vertex. In this case, the average number of nucleation sites per cubic particle is

$$A = 8\left(\frac{R}{d}\right)^2 \tag{4}$$

Thus the crystallised volume fraction is

$$\alpha(t) = \frac{A}{8}\left(\frac{ut}{R}\right)^3 \tag{5}$$

In this case, $\alpha(t)$ evolves until $r_m = ut_m = 2R$, when total surface transformation occurs at t_m. The usefulness of this simple model was demonstrated for surface induced crystallisation of cordierite glass powders.[6]

The classical model of Johnson, Mehl, Avrami & Kolmogorov[9–13] describes the transformation kinetics of some given area or volume, which is given by

$$\alpha(t) = 1 - \exp\left[-\alpha*(t)\right] \tag{6}$$

where $\alpha*(t)$ is the fictitious extended area or volume, i.e. the total fraction transformed without taking into account the overlapping of the growing units. $\alpha*(t)$ can be calculated for several geometries.

Using this equation, Gutzow *et al*[8] proposed a way to describe the kinetics of overall crystallisation of powdered glasses. They assumed a fixed concentration N_s of nucleation sites on the surface of spherical particles having radius R, and that the process occurs in two main stages. In the initial stage, three dimensional growth of semi-spherical crystals from the surface leads to

$$\alpha*(t) = \frac{2\pi N_s u^3 t^3}{R} \tag{7}$$

with growth spreading over the particle surfaces and towards their interior. After some critical period of time, further growth on the surface is limited because the crystals impinge. They thus stop growing on the surface and only those whose fastest growing direction is perpendicularly oriented to the glass grain surface keep growing towards the particle interior. After this intermediate period of crystal selection, a final stage starts when cylindrical crystals grow perpendicularly from the surface towards the glass grain centre. The extended volume transformed of such cylindrical crystals is given by

$$\alpha*(t) = \frac{3\pi ut}{4R} \tag{8}$$

Equation (8) was derived considering a regular and quadratic array of nucleation sites on the surface of the particles. Semi-spherical crystals could start growing from them and would impinge at a period

of time, t_m, given by

$$t_m = \frac{1}{2u\sqrt{N_s}} \tag{9}$$

At t_m the crystallisation kinetics change from that of Equation (7) to that of Equation (8). Considering the quadratic array of crystals supposed by Gutzow *et al*,[8] we estimate that the surface of the glass particles would be about 80% crystallised at t_m.

Vázquez *et al*[14] performed a derivation similar to that of Gutzow *et al*,[8] but instead of considering that the extended volume of cylindrical crystals is given by Equation (8), for the final stage of crystal growth they considered

$$\alpha*(t) = \frac{3ut}{R} \tag{10}$$

that starts at

$$t_m = \frac{1}{u\sqrt{\pi N_s}} \tag{11}$$

Equations (10) and (11) are obtained supposing a circular section through the centre of spherical glass particles with equidistant semicircular crystals having the centre on the particle surface and growing towards the particle centre. At impingement, the crystals have maximum diameter, $2r_m$. However, this situation can not be generalised to 3-dimensions (3D). The resulting numerical value for t_m differs from that of Gutzow by a factor $[\sqrt{\pi}]/2$.

Theory

In the present work we also assume semi-spherical crystals nucleated on athermal sites on the surface N_s of spherical glass particles of radius R, which grow towards the particle centres, as did Gutzow *et al*[8] and Vazquez *et al*[14] for the first stage of crystallisation. The adequate expression to describe this stage is Equation (7). Later on the crystals impinge and occupy the particles surface.

We then consider a second stage with prismatic crystals growing inwards the glass grain centre. An expression for this stage is derived below. Considering glass particles with prismatic crystals having their longitudinal axis normal to the particle surface and that grow inwards the bulk, if the nuclei density is so high that a crystallised layer covers the particles ($d \ll R$), an expression for the extended volume is

$$\alpha*(t) = \frac{V_c}{V_p} = \frac{3na_c ut}{NS_p R} \tag{12}$$

where V_c is the (extended) crystallised volume, V_p the volume of particles, n the number of crystals or nucleation centres on the particles surface, a_c the base area of each prismatic crystal of height (ut) growing in the bulk, N is the number of glass particles in the

assembly, and S_p is the surface area of one particle (thus NS_p is the total glass powder surface area). An estimate of the prism base area a_c is

$$a_c = \frac{S_c}{n} \tag{13}$$

where S_c is the crystallised area on the particle surface, and n is the number of nucleation centres on the same surface. In this way we are also assuming a uniform distribution of crystals on that surface. If

$$N_s = \frac{n}{NS_p} \tag{14}$$

and the surface crystallised fraction as is given by

$$\alpha_s = \frac{S_c}{NS_p} \tag{15}$$

substituting Equations (14) and (15) into Equation (13) one arrives at

$$a_c = \frac{\alpha_s}{N_s} \tag{16}$$

Substituting Equations (14) and (16) into Equation (12), the extended volume can be approximated by

$$\alpha^*(t) = \frac{3\alpha_s u t}{R} \tag{17}$$

The maximum time interval, t_m, for 3D growth, i.e. in Equation (6) when the growth kinetics change from that given by Equation (7) to that given by the Equation (17), can be estimated knowing the growth velocity of crystals on the particle surface, as follows.

The surface fraction of circular crystals during the 3D growth stage, α_s, is given by the JMAK expression

$$\alpha_s(t) = 1 - \exp\left(-\pi N_s u^2 t^2\right) \tag{18}$$

To exactly calculate t_m we should make $\alpha_s(t_m)=1$ in Equation (18) and solve it for t, but this procedure does not yield a solution. We thus consider $\alpha_s(t_m) \approx 1 - d\alpha_s$, where $d\alpha_s$ is a small fraction remaining to achieve total crystallisation of the particle surface, such that in the limit, when $d\alpha_s \rightarrow 0$, $\alpha_s(t_m) \rightarrow 1$. We can then assume a practical $d\alpha_s$ remaining to achieve total crystallisation (e.g. as small as 1%). In doing that, from Equation (18) we have

$$t_m = \sqrt{\frac{\ln d\alpha_s}{-\pi N_s u^2}} \tag{19}$$

In this way, we assume that the surface of each particle is almost totally occupied by crystals that started growing on that surface in a circular mode. Herein in the text we will refer to this approach as the *semi-spherical model.* To further extend the crystallisation kinetics proposed in this work, cylindrical crystals can be supposed to grow from the beginning of crystallisation, and then we only need Equations

(6), (17) and (18) for the whole kinetics. In this way it is not necessary to consider the changing kinetics from 3D to 1D growth mode and calculate the time interval for the crystals to impinge, t_m. Herein in the text we will refer to this second approach as the *cylindrical model.*

Based on the above described assumptions, our aim is thus to obtain N_s for a powdered glass. In our approach one needs to know the crystal growth rate at the heat treatment temperature, u, and the volume fraction crystallised, $\alpha_v(t)$. We then compare ours with previous approaches.

2. Experimental

A glass having the stoichiometric composition of diopside ($CaO.MgO.2SiO_2$) was prepared by mixing the correct proportion of high grade chemicals. We use diopside as a suitable model glass, due to: (i) the high confidence we have on the values of crystal growth rate (u) as a function of temperature for this system and the insensitivity of u to small compositional differences between different glass melts;[15] (ii) because only one crystal phase develops on heating; and (iii) because of its high chemical durability, which prevents formation of extra nucleation sites (by chemical attack) after sample preparation.

The chemicals were mixed in a Fritsch Pulverisette 6 high impact mill with Si_3N_4 jar and balls. The batch was then melted in a Pt crucible at 1500°C for 4 h. The liquid was poured into a stainless steel mould and let to cool down in air. Minor devitrification patches formed on the surface of the glass plaque, which were ground off. The glass block was hammered and the ground pieces were further milled in the high impact mill for short time periods (30 s at 350 rpm) to keep the particle sizes in the desired range without introducing too many defects on the newly created surfaces. The glass powder was sieved through a 38–75 μm polymer mesh. The collected powder was washed in water to eliminate most of the fine particles that usually attach to the coarse ones.

To prepare compacts for sintering the collected powder was mixed with 20 wt% oleic acid. This powder was subsequently heated to 500°C for some seconds to remove the excess acid, acquiring a gray colour, which indicated that burning was only partial and that some residue remained. We proceeded in this way to enhance particle packing when pressing the powder into discs. Approximately 25 mg of powder were pressed under 2500 kgf in a stainless steel die into 1·5 mm thick discs having 10 mm in diameter. The acid was totally eliminated by subsequently heating the samples at 500°C for 1 h, resulting in white discs. Two sets of samples were independently produced following the above procedure. The samples were labelled *D, E, F, G, H,* and *I,* each

letter indicating a particular position in the sample holder during heat treatment in an attempt to test its possible effect, which was afterwards considered insignificant. The samples *D, E, F* originated from a different batch from *G, H, I*. The samples *D, E, F* were heat treated together; the same is true for set *G, H, I*. The crystallised fraction for samples *G, H, I* was only determined by XRD.

All these samples were heat treated at 825°C, for 30 min to 8 h, for simultaneous sintering and crystallisation. For each sintering experiment the samples were heated together. It should be stressed that the change in the crystal/glass front temperature due to the release of the crystallisation heat, as given by the expression of Herron & Bergeron[16] is not important at this temperature for diopside.

The sintered discs were sectioned through half the diameter and one of the sectioned faces was polished for microscopy. We used a Leica DMRX optical microscope having digital image capture and a Zeiss KS200 software for image analysis. Ten images of each section, randomly taken, were analysed. Samples treated for time periods shorter than 2 h presented too thin surface crystallised layers, and it was thus difficult to analyse them in an optical microscope. Therefore, such samples were only analysed by XRD to estimate their crystallised volume fraction.

The experimental crystallised volume fraction $\alpha_v(t)$ relative to the solid part (without taking the pores into account) was determined by measuring the porosity $P(t)$ and the crystallised fractions $C(t)$ in the micrographs, as given below

$$\alpha_v(t) = \frac{C(t)}{1 - P(t)} \qquad (20)$$

By using a square grid, the parameters $C(t)$ and $P(t)$ were determined counting the number of intersections of horizontal and vertical lines within the crystallised and porous phases, respectively, and dividing the results by the total number of points of the grid.

Although this method can give precise results, it requires several micrographs and is quite time consuming. Alternatively, x-ray diffraction has the advantage of sampling a large area on a single test, allowing a rapid determination of $\alpha_v(t)$. There are several XRD techniques for quantitative determination of phase proportions in multicomponent glass-ceramics, as reviewed by Kim *et al*.[17] Here we used a calibration curve by measuring the intensity of a particular diopside line in a set of calibration samples having known crystallised volume fractions.

The calibration samples were obtained by weighting determined amounts of glassy and crystallized diopside, m_g and m_c, respectively, both powders having particle diameters smaller than 22 μm, in a Mettler Toledo AX 204 balance accurate to 0·1 mg. The

Table 1. Diopside glass weight (m_g) and crystallised diopside weight (m_c) in the XRD calibration samples, weight fraction crystallised (X_c) and volume fraction crystallised (α_v)

Sample	m_g (g)	m_c (g)	X_c (%)	α_v (%)
CS-1	0·1590	0	0·00	0·0
CS-2	0·1423	0·0076	5·07	4·4
CS-3	0·1225	0·0136	9·99	8·7
CS-4	0·1176	0·0306	20·64	18·3
CS-5	0·1074	0·0447	29·39	26·4
CS-6	0·0903	0·0600	39·92	36·4
CS-7	0·0760	0·0764	50·13	46·4
CS-8	0·0624	0·0926	59·74	56·1
CS-9	0·0487	0·1064	68·60	65·3
CS-10	0·0227	0·1278	84·92	82·9
CS-11	0	0·1772	100	100·0

crystallized diopside powder was obtained by heat treating at 825°C for 10 h part of the diopside glass powder with diameters under 22 μm. That resulted in a sintered compact, which was then milled in the high impact mill. The glassy and crystallised powders mixed at calculated proportions to form the calibration samples were homogenised in an agate mortar and pestle with isopropyl alcohol. After drying in an oven at 100°C the mixtures were hand pressed in an agate mortar with the pestle to break the aggregates to obtain a fine, homogeneous powder. The calibration samples were weighted to give enough mass to fill the XRD sample holder. The resulting masses are shown in the Table 1.

We used a Siemens D5005 XRD operated at 40 kV and 40 mA. The spectra for each calibration sample and afterwards for the samples having unknown crystallised fractions were determined for 2θ from 28° to 32°, with step size of 0·0250° and measurement time period of 10 s for each step. We then determined the intensity of the most intense diopside peak, relative to the $(\bar{2}21)$ plane that diffracts at $2\theta = 2·781°$ (JCPDF 86-0932).[18,19] Its position varied in our experiments from 29·800° to 29·850°. The peak intensity was determined from a straight line that was built by linking the average background intensity at 29·125° and 31·500°.

The crystallised volume percent, α_v of the calibration samples were calculated by using the diopside glass and crystal densities, respectively ρ_g and ρ_c, following Equation (21). The results are shown in Table 1

$$\alpha_v = \frac{m_c \rho_c}{\left(m_g \rho_g + m_c \rho_c \right)} 100 \qquad (21)$$

The glass density was measured by the Archimedes method using a Mettler Toledo AX 204 balance coupled with a kit for density measurement. The diopside crystal density was obtained from the literature.

Half of the sintered discs that were not used for microscopy were powdered in an agate mortar and
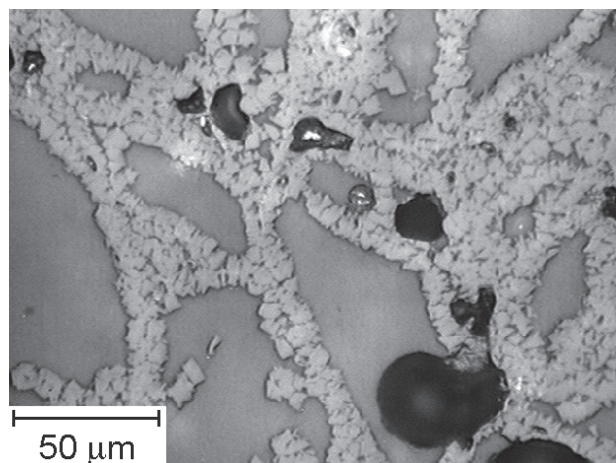
Figure 1. Micrograph of a polished cross section of a sample heat treated for 4 h at 825°C

Figure 2. Particle distribution before and after pressing the glass powder into discs

pestle to pass completely through a 22 μm nylon sieve. Unfortunately, most of the obtained sample masses were not enough to completely fill the XRD sample holder. To avoid underexposure of the samples to the x-rays, we added a known mass of diopside glass particles, with 22 μm in diameter, to complete the amount needed to fill the sample holder (around 0·15 g). Precisely weighted amounts of sintered and glassy powders were mixed in an agate mortar and pestle with isopropyl alcohol and dried. To account for the crystallised fraction, α_v, of the sample before adding more glass, we corrected the crystallised volume fraction obtained from the calibration curve, F_v, through the equation

$$\alpha_v = \frac{F_v \rho_g \left(m_{ag} + m_s \right)}{m_s \rho_g + F_v m_{ag} \rho_g - F_v m_{ag} \rho_c} \qquad (22)$$

where m_{ag} is the mass of glass added and m_s is the mass of the sintered sample. One can see that when m_{ag} is zero, $\alpha_v = F_v$.

3. Results and Discussion

The JCPDF card no. 86-0932[18,19] closely fits the powder diffraction pattern of the totally crystallised sample. The density of crystalline diopside from that JCPDF card is 3·261 g/cm^3. Our measured density for a non-annealed diopside glass piece was 2·805±0·005 g/cm^3 (within 95% confidence limits).

Figure 1 shows an example of the microstructure of a heat treated sample. This figure shows sectioned sintered grains whose centres are still glassy but their surfaces have crystallised. The thickness of the crystallised surface layer increased with the time interval of heat treatment time up to a point when the glass grains were completely consumed by the crystals. A significant amount of spherical pores appear inside the grains, especially after the longest heat treatments, which can be a result of degassing (i.e. dissolved gases in the glass grains come out
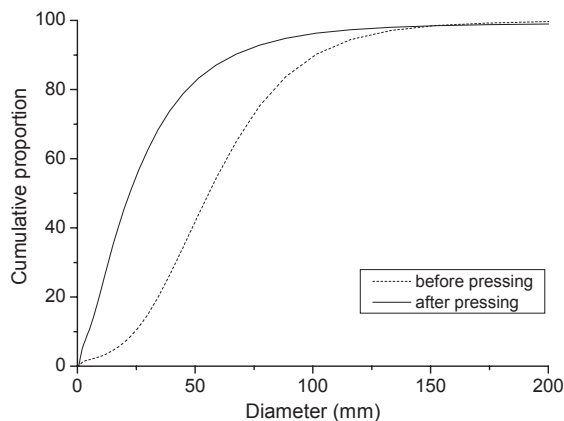
during crystallisation) and large mismatch between the diopside glass and crystal densities. Other pores with irregular shapes indicate that full densification through viscous flow sintering is hindered by surface crystallisation.

Figure 1 confirms that the original glass grains are not spherical and have a size distribution, thus deviating from the assumptions of the theoretical models used here. The particle size distribution of the powder used was between 38 μm and 75 μm, and thus, nominally, it has "diameters" within such range. Nevertheless, the experimental size distributions of the powders before and after pressing in a die were characterised in a Horiba LA-930 laser scattering particle size analyser. The after pressing powder was obtained by gently pulverising a pressed disc and washing it into water. For measuring, suitable suspensions were prepared in water by adding one drop of a deflocculating agent and letting the materials under ultrasound waves for 10 min. The results are shown in Figure 2.

Figure 2 shows that the initial powder (before pressing) had average diameter of 56 μm, and agree with the nominal average aperture of the sieves. However, the diameters of such powder range from under 38 μm to over 75 μm, reaching approximately 150 μm. This is probably because some particles had high *aspect ratio* (the ratio between the largest and smallest diameters), in such way that the smallest diameter of the particle passed through the 75 μm sieve, but the largest one was so large that, in average, such particles show equivalent spherical diameters over 75 μm.

Figure 2 also shows the particles fractured during pressing into discs at 320 MPa. The size distribution still ranges from zero to approximately 150 μm, but the average diameter decreased to 22 μm after pressing. Efforts to simplify the experimental procedure by using mono-size glass beads are in progress.

Table 2 shows results of α_v determined by microscopy (α_v MIC) and the associated error (Eα_v MIC

Table 2. Sintered sample parameters: sample names indicating the sintering time interval in hours and sample label (D,E,F,G,H or I); sample weight (m_s); added glass weight (m_{ag}); XRD ($\bar{2}21$) peak intensities (I); crystallised volume fraction from the XRD calibration curve (F_v); crystallised volume fraction from the XRD calibration curve after correcting for the added glass (α_v XRD); crystallised volume fraction from microscopy (α_v MIC); and respective crystallised volume fraction errors (EF_v, $E\alpha_v$ XRD, $E\alpha_v$ MIC)

Sample	m_s	m_{ag}	I	F_v	EF_v	α_v XRD	$E\alpha_v$ XRD	α_v MIC	$E\alpha_v$ MIC
	(g)	(g)	(cps)	(%)	(%)	(%)	(%)	(%)	(%)
0·5/G	1*	0	69	1	3	1	3	-	-
0·5/H	1*	0	82	2	3	2	3	-	-
0·5/I	1*	0	59	1	3	1	3	-	-
1/G	1*	0	189	6	3	6	3	-	-
1/H	1*	0	218	7	3	7	3	-	-
1/I	1*	0	211	7	3	7	3	-	-
2/G	1*	0	700	27	3	27	3	-	-
2/H	1*	0	739	28	3	28	3	-	-
2/I	1*	0	691	26	3	26	3	-	-
4/D	0·1042	0·0493	1339	53	3	81	4	71	6
4/E	0·0634	0·0860	842	32	3	83	7	83	7
4/F	1*	0	1875	74	3	74	3	70	9
4/G	1*	0	1596	63	3	63	3	-	-
4/H	1*	0	1581	62	3	62	3	-	-
4/I	1*	0	1526	60	3	60	3	-	-
6/D	1*	0	2269	90	3	90	3	88	6
6/E	0·0933	0·0608	1384	54	3	96	5	92	2
6/F	0·0736	0·0757	1129	44	3	97	6	91	3
8/D	0·0495	0·1037	776	30	3	103	10	95	2
8/E	0·0758	0·0893	1029	40	3	95	7	94	3
8/F	0·0659	0·0887	894	35	3	88	7	95	3
10/D	0·0568	0·1528	631	24	3	99	12	95	3
10/E	1*	0	2350	94	3	94	3	97	4
10/F	0·0728	0·0712	1237	48	3	104	6	98	2

* We considered m_s=1 g and m_{ag}=0 g when no glass was added to complete the sample

– within 95% confidence interval for the average). Figure 3 shows the crystallised volume fraction of the calibration samples, obtained by Equation (21), as a function of the XRD peak intensity after baseline correction. One observes that α_v of the calibration samples follow a straight line with the XRD peak intensities. The prediction limits, shown in the graph, are approximately ±3 vol% for any crystallised volume fraction predicted by the linear model: $F_v=A+BI$, where I (counting per second, cps) is the maximum intensity of the peak at around $2\theta=2\cdot825°$, $A=-1\cdot60422$
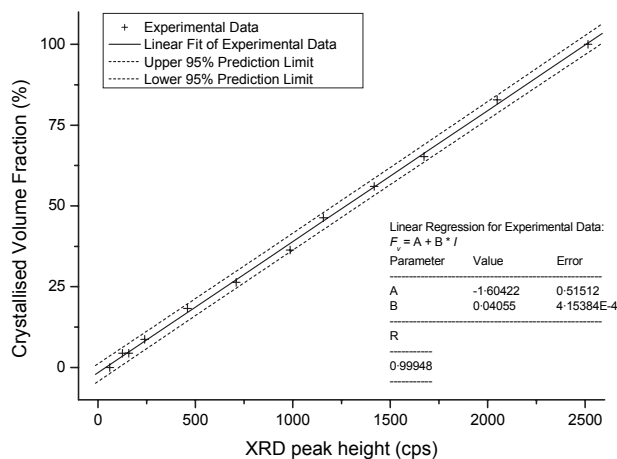

Figure 3. Calibration curve for the diopside ($\bar{2}21$) XRD peak. Peak intensity for several standard samples having different crystallised volume fractions

and $B=0\cdot04055$ are regression constants.

The crystallised volume fraction, F_v, obtained by measuring by XRD and substituting the value in the calibration curve of Figure 3, are also shown in Table 2, together with the respective 95% error, EF_v. Table 2 also shows the masses of the sintered compacts and of glass powder used to prepare the XRD samples. These data inserted into Equation (22) resulted in the crystallised volume fractions for the sintered samples, α_v XRD, shown in the Table 2. The error in the α_v XRD values, $E\alpha_v$ XRD, was estimated considering that it only depends on the error in F_v, despite additional errors in m_{ag}, m_s, ρ_g and ρ_c, and making

$$E\alpha_v XRD = \frac{\partial \alpha_v}{\partial F_v} EF_v \qquad (23)$$

where α_v is given by the Equation (22). The results for $E\alpha_v$ XRD are shown in Table 2.

The preparation of XRD samples by adding a known mass of diopside glass to the sintered powder induces high errors. The correctness of this procedure was checked by measuring F_v in additional samples (that had enough mass) before and after adding more glass to them. In the first case $\alpha_v=F_v$ and in the second α_v is given by Equation (22). The results are shown in Table 3, the samples having added glass are labelled 2 after identification. One observes that for samples 4/F and 10/E the results with and without added glass closely agree. However, samples 6/D,

Table 3. Identical parameters of Table 2 for pure samples and after mixing to a given mass of added glass (identified by "2" after the sample label)

Sample	m_s	m_{ag}	I	F_v	EF_v	α_v XRD	$E\alpha_v$ XRD	α_v MIC	$E\alpha_v$ MIC
	(g)	(g)	(cps)	(%)	(%)	(%)	(%)	(%)	(%)
4/F	1*	0	1875	74	3	74	3	70	9
4/F2	0·0837	0·0772	944	37	3	75	6		
6/D	1*	0	2269	90	3	90	3	88	6
6/D2	0·0951	0·1838	821	32	3	103	9		
10/E	1*	0	2350	94	3	94	3	97	4
10/E2	0·0891	0·0624	1294	51	3	92	5		

* We considered m_s=1 g and m_{ag}=0 g when no glass was added to prepare the sample

which had an exaggerated glass mass added, aiming to test this effect, present the highest deviation and error, indicating that the error is dependent of the fraction of glass added. By plotting the $E\alpha_v$ XRD (%) as a function of the mass fraction of added glass [$m_{ag}/(m_s+m_{ag})$] (Figure 4), one clearly observes that the error increases as this fraction increases. But, in general, the results of crystallised volume fraction determined by microscopy and XRD agree within the error limits (Table 2).

The reproducibility of the XRD measurements was also evaluated by repeating the test for two additional samples, labeled 2/B and 8/C, whose α_v XRD presented high deviation from α_v MIC (results not presented). Table 4 shows the results, where the replicas are labelled *b*. The α_v XRD repeatability, $\Delta\alpha_v$ DRX (the difference between α_v XRD for the sample and the replica), was sufficient for the aims of the present work.

The good agreement between the results of XRD and microscopy confirms the crystallised volume fractions determined in the present work. The results from microscopy, however, look more consistent because they never reach 100 vol%, which occurs for the XRD technique due to its inherent errors. From now on, we take the XRD and the microscopy data to estimate N_s using all crystallisation models presented in the Introduction.
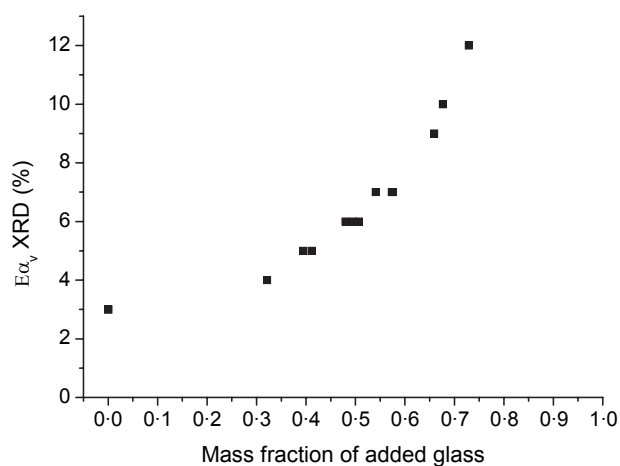
Figure 5 shows the experimental volume fraction

Table 4. Identical parameters of Table 2 for samples measured twice (the replica is identified by "b" after the sample label). The difference between two α_v XRD is shown as $\Delta\alpha_v$ DRX

Sample	m_s (g)	m_{ag} (g)	I (cps)	F_v (%)	EF_v (%)	α_v (%)	$E\alpha_v$ XRD (%)	$\Delta\alpha_v$ DRX (%)
2/B	0·0765	0·0752	754	29	3	60	6	2
2/Bb	0·0765	0·0752	729	28	3	58	6	
8/C	0·0367	0·1145	638	24	3	114	14	1
8/Cb	0·0367	0·1145	632	24	3	113	14	

crystallised in sintered diopside glass-ceramic compacts as a function of the time interval at 825°C. We omit the error bars for simplicity. Part of the potential experimental variation could be eliminated by heat treating the samples together, but the results can be strongly affected by the surface condition of the particles, whose effect on N_s has been reported.[20]

To test the effect of oleic acid on the surface crystallisation kinetics of the glass particles, we measured the crystallisation peak by differential scanning calorimetry (DSC) as a function of temperature of powders treated with and without oleic acid. DSC can be used to gauge the crystallisation tendency of glasses [e.g. Ref. 21]. To exaggerate the effect of oleic acid, 0·25 g of glass powder were soaked in 0·25 g of

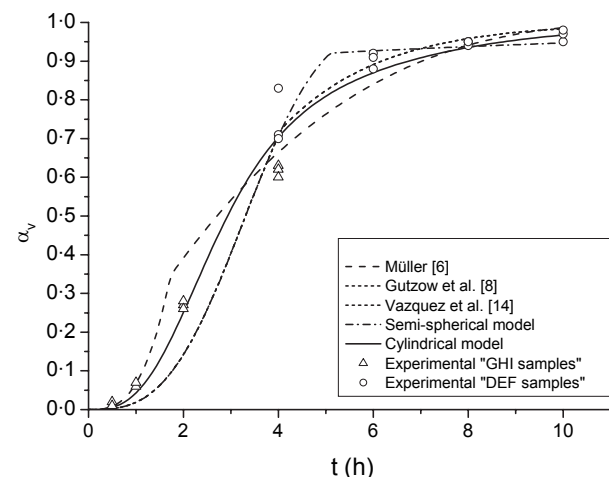*Figure 4. $E\alpha_v$ XRD (%) as a function of the mass fraction of added glass*

Figure 5. Experimental volume fractions crystallised in sintered diopside glass compacts as a function of the time interval at 825°C (triangles and circles). Curve fits of different expressions to the experimental data (lines)

Table 5. DSC characteristic temperatures of the crystallisation peaks of oleic acid treated and untreated samples

Sample	$T_{c\,onset}$ (°C)	$T_{c\,max}$ (°C)
Untreated powder	876	906
Untreated powder	877	907
Treated powder	876	910

Table 6. Resulting N_s, *R, and regression coefficients* (r^2) *from the different models*

Author	$N_s \times 10^{10}$ (m^{-2})	R (μm)	r^2
Muller	16±8	9·4±0·4	0·97
Gutzow *et al*	3±1	3·6±0·5	0·97
Vazquez *et al*	4±1	4·5±0·7	0·97
Semi-spherical model, this work	22±2	30±2	0·97
Cylindrical model, this work	8±2	6·3±0·4	0·99

oleic acid (enough to immerse the powder into the acid) for 25 h at room temperature. After this time, the acid was poured away and the powder was heated up at 10°C/min to approximately 500°C, left at this temperature for 2 h, and subsequently cooled down in the furnace. A Netzsch DSC 404 was used to get the DSC curve by heating at 10°C/min to 1000°C. The DSC curve for the untreated sample was measured twice to evaluate the DSC repeatability. The onset ($T_{c\,onset}$) and the maximum ($T_{c\,max}$) temperatures of the crystallisation peak were obtained from the resulting curves (not shown).

The characteristic temperatures of crystallisation shown in Table 5 indicate that the crystallisation behaviour of acid treated and untreated glass are about the same. Thus we can disregard the effect of oleic acid and consider the different powder granulometry after pressing (effect shown in Figure 2) as the main source of the data scatter observed in Figure 5.

Despite the significant scatter, Figure 5 shows that, on average, the experimental volume fraction crystallised increases with the time period at 825°C, and achieves about 100% after 10 h of heat treatment at this temperature. The micrograph of Figure 1 shows that there are many crystals on the particle surfaces, and thus $d<R$. We then considered Muller's model for $d<R$, given by Equations (1) to (3). Allowing only d or N_s as a free parameter to fit the models to the experimental data, we do not always obtain a good fit. We thus let d and R act as free parameters to fit to Muller's model, and N_s and R as free parameters to fit to the other models. One may expect a variation of N_s with particle size (for instance, the smallest particles may have more surface defects per unit area than the largest particles). In our approach we determine an average value of N_s for all particle sizes. By comparing R from the fittings with the experimental values (Figure 2), one can check the resulting parameters and evaluate the different models.

The continuity of each function of the crystallised volume fraction as a function of the time interval of transformation forces the crystallised volume fraction to have the same value at tm calculated by the 3D and the 1D crystallisation expressions. To account for this, we first calculate $\alpha_v(t_m)$ using the expression for each model in the 3D stage, using t_m calculated by the corresponding expression. We then calculate the time t_0 to achieve the thus obtained $\alpha_v(t_m)$, considering the expression for each crystallisation model in the 1D stage. The crystallised volume fraction values are further obtained making $t=t+t_0-t_m$ in $\alpha_v(t+t_0-t_m)$, using

the respective expression of each different model in the 1D stage, such that when $t=t_m$, $\alpha_v(t_m)=\alpha_v(t_0)$. In the special case assumed by Muller,[6] $t_m=t_0$.

Figure 5 shows several curves calculated by the different models described in the Introduction, including ours, fitted to the experimental data letting d or N_s and R as free parameters. We used $u(825°C)=2\times10^{-10}$ m/s and $d\alpha_s=0·0001$. Our *cylindrical model* best fits the experimental data. The poor fit of the experimental data to the other models, especially for small crystallised fractions, probably arises due to finite size effects, as demonstrated by Levine *et al*.[22] Muller's model best fits the very beginning of crystallisation.

The fittings with the models of Gutzow *et al*[8] and Vazquez *et al*[14] coincide within the error limits. The resulting N_s and R for each case are given in Table 6. In the case of Muller's model, N_s is calculated from d and R, using the following expression deduced from his assumed geometry

$$N_s = \frac{1}{4d^2} + \frac{1}{12R^2} \tag{24}$$

Table 6 shows that the resulting value of R from the semispherical model is larger than the average radius (after pressing), which is approximately 11 μm, from Figure 2. From Muller's model $R=9·4±0·4$ μm and this is thus the one that best estimates the experimental average radius. However, the results for R and N_s from the *semi-spherical model* depend of the choice of $d\alpha_s$. Table 7 shows values for R and N_s calculated using the *semi-spherical model* for different $d\alpha_s$, from 1% to 1 ppm. Using the experimental R to gauge $d\alpha_s$ in that model, one can see that considering 1% residual glass on the particles surface, the fitted R closely agrees with the experimental value. With $d\alpha_s$ in such level, the *semi-spherical model* and Muller's model closely agree. This result gives a consistency test for the geometry and calculation procedure proposed here and by Muller.[6]

Nevertheless, the values of R obtained by the other models are not too discrepant, but fall slightly below the expected range. This small discrepancy could perhaps be taken into account if we recall that the glass particles have a relatively wide size distribution and their shape is not spherical. The models from Gutzow *et al*, Vazquez *et al* and our semispherical model have near the same $\alpha(t)$ behaviour. An explanation for this result probably rests on Equation (6).

Table 7. Resulting N_s *and* R *from the semi-spherical model for different fractions of residual glass on the surface of the particles when the growth mechanism changes*

$d\alpha_s$	R *(µm)*	$N_s \times 10^{-10}$ *(m⁻²)*
0·01 (1%)	10±2	12±2
0·001	20±2	17±2
0·0001	30±3	22±3
0·00001	30±3	27±3
0·000001 (1 ppm)	40±4	32±4

Besides different extended volumes (α^*) considered, different u, R or N_s have a stronger effect than the geometries of the crystals and glass particles assumed. Despite the slightly smaller R, the experimental data for $\alpha_v(t)$ is best described assuming cylindrical crystals growing from the beginning of the crystallisation (*cylindrical model*), as shown by the respective curve in Figure 5.

The values of N_s from Muller's model and the two models presented here (considering $d\alpha_s$=1% for the *semi-spherical model*) closely agree into the error limits. But N_s from the models of Gutzow *et al* and Vasquez *et al* are only slightly smaller. The N_s values calculated here have the same order of magnitude than those for a cordierite glass powder (10^9 to 10^{11} m⁻²).[23]

Unfortunately, optical determination of N_s is a very difficult and not practical task, especially in the case of small jagged particles prepared for sintering (as in the present case). That is exactly why we and other authors came up with some models that allow an indirect estimation of N_s. In this paper we found reasonable agreement between experimental and fitted average R and compared then to check the models. We are now in an advanced stage working on directly measuring N_s on sintered and partially crystallised glass particle compacts by optical microscopy, this way keeping intact the processing effects on N_s. We will publish the results presently.

4. Conclusions

The models of Muller, Gutzow *et al*, Vazquez *et al* and ours are more sensitive to N_s, R, and u than to the crystal and glass particle morphology. This fact explains why all these different models work relatively well. The models of Gutzow *et al* and Vazquez *et al* show almost the same behaviour, and give the same N_s, within the error limits. Our model with cylindrical crystals growing from the beginning to the final stages of crystallisation best fits the experimental data, and the resulting N_s and R are not too discrepant from the other models.

Overall, all the methods allow one to estimate N_s with reasonable accuracy. Our methods provide a step forward for modelling heterogeneous nucleation on glass particles surface because they do not assume any geometrical arrangement of nucleation sites on the surface. Additionally, our *cylindrical model* has a unique equation and does not need to account for changing growth mechanisms from 3D to 1D.

5. Acknowledgements

6. References

1. Höland, W., Rheinberger, V., Apel, E. & van't Hoen C. *J. Eur. Ceram. Soc.,* 2007, **27**, 1521.
2. Höland, W. & Beall, G. H. *Glass-ceramic Technology*. John Wiley & Sons, Am. Ceram. Soc., Westerville, 2002.
3. Zanotto, E. D. & Prado, M. O. *Phys. Chem. Glasses,* 2001, **42**, 191.
4. Mampel, K. *Z. Phys. Chem.,* 1940, A 187, **43**, 225.
5. Todes, K. M. *Zh. Fiz. Khim. (URRS),* 1940, **14**, 1224.
6. Muller, R. *J. Therm. Anal.,* 1989, **35**, 823.
7. Grimshaw, R. W. *The Chemistry and Physics of Clays and Allied Ceramic Materials*. Ernest Benn, London 1971, 667.
8. Gutzow, I., Pascova, R., Karamanov, A. & Schmelzer, J. *J. Mater. Sci.,* 1998, **33**, 5265.
9. Johnson, W. A. & Mehl, R. F. *Trans. AIME,* 1939, **135**, 416.
10. Avrami, M. *J. Chem. Phys.,* 1939, **7**, 1103.
11. Avrami, M. *J. Chem. Phys.,* 1940, **8**, 212.
12. Avrami, M. *J. Chem. Phys.,* 1941, **9**, 177.
13. Kolmogorov, A. *Izv. Acad. Sci. URSS Ser. Math.,* 1937, **1**, 355.
14. Vazquez, J., Garcia, G., Barreda D., Lopez-Alemany P. L., Villares, P. & Jimenez-Garay, R. *Thermochim. Acta,* 2005, **430**, 173.
15. Nascimento, M. L. F., Ferreira, E. B. & Zanotto, E. D. *J. Chem. Phys.,* 2004, **121**, 8924.
16. Herron, L. W. & Bergeron, C. G. *Phys. Chem. Glasses,* 1978, **19**, 89.
17. Kim, H. S., Rawlings, R. D. & Rogers, P. S. *Br. Ceram. Trans. J.,* 1989, **88**, 21.
18. JCP 86-0932 EVA Application 7,0,0,1 SOCABIM ®.
19. Harlow, G. E. *Am. Miner.,* 1996, **81**, 632; in the JCPDF 86-0932.[18]
20. Muller, R. *J. Non-Cryst. Solids,* 1997, **219**, 110.
21. Ray, C. S., Day, D. E., Huang, W., Lakshmi Narayan, K., Cull, T. S. & Kelton, K. F. *J. Non-Cryst. Solids,* 1996, **204**, 1.
22. Levine, L. E., Lakshmi, K. & Kelton, K. F. *J. Mater. Res.,* 1997, **12**, 124.
23. Muller, R., Reinsch, S., Sojref, R. & Gemeinert, M. *Proc. XVII Int. Congr. on Glass,* Beijing, 1995, **5**, 564.